THESIS

DECODING DEEP CONVECTION: LINKING CLOUD TOP COOLING TO ENVIRONMENTAL CONDITIONS AND STORM EVOLUTION

Submitted by

Thomas M. Juliano

Department of Atmospheric Science

In partial fulfillment of the requirements

For the Degree of Master of Science

Colorado State University

Fort Collins, Colorado

Fall 2025

Master's Committee:

Advisor: Steven Miller
Co-Advisor: Jason Apke

Kristen Rasmussen
Haonan Chen

ABSTRACT

DECODING DEEP CONVECTION: LINKING CLOUD TOP COOLING TO ENVIRONMENTAL CONDITIONS AND STORM EVOLUTION

Forecasting severe deep convection (DC) remains a critical challenge in atmospheric science, particularly during the early stages of storm development when traditional radar-based methods may lack sensitivity. This study explores the use of optical flow (OF)-based cloud-top cooling (CTC) as a diagnostic tool for identifying and characterizing DC initiation, environments, and subsequent evolution. By analyzing 1,063 convective events from the 2024 spring storm season from a satellite, radar, and numerical model perspective, this research evaluates the relationship between CTC intensity and environmental instability, as well as the timing of significant and severe storm development. The results demonstrate that stronger CTC signals are generally associated with more unstable atmospheric conditions and are often observed prior to the onset of radar-detectable storm features. These signals tend to precede both the initial development of DC and the emergence of severe weather indicators, such as large hail, by lead times that decrease with increasing CTC magnitude. Integrated CTC metrics, which capture the persistence of cooling over time, further enhance the ability to distinguish between transient and sustained convective systems. While variability exists due to environmental complexity and observational limitations, the findings suggest that CTC offers a meaningful and operationally relevant approach to understanding updraft intensity and near-term evolution. Future efforts will focus on expanding the temporal scope of analysis and integrating additional indicators also tracked with OF to refine the predictive capability of CTC-based diagnostics.

ACKNOWLEDGEMENTS

Funding was provided by NASA Grant # 80NSSC21K0919 and the Colorado State University Walter Scott Jr. College of Engineering.

TABLE OF CONTENTS

1 INTRODUCTION

According to the National Oceanic and Atmospheric Administration (NOAA) National Centers for Environmental Information (NCEI), Severe Deep Convection (DC) produces numerous “billion-dollar” disasters in the United States annually, posing significant threats to life, property, and infrastructure (NOAA NCEI 2025). Despite substantial advancements in numerical weather prediction (NWP), radar systems, and satellite remote sensing, the accurate diagnosis and short-term forecasting of severe convection remains a persistent challenge in atmospheric science (Line et al. 2015) . One of the key limitations in current forecasting systems is the difficulty in observing the early, non-precipitating stages of storm development. While radar excels at detecting precipitation and mature storm structures, it often misses the initial vertical growth of convective clouds (Adler and Fenn 1979). Satellite-based methods, particularly those using infrared (IR) channels, offer a unique advantage by continuously monitoring cloud-top temperatures and structure. Among these, cloud-top cooling (CTC) has emerged as a valuable early signal for nowcasting convective initiation (CI; Mecikalski and Bedka 2006). However, traditional objective CTC retrievals are often noisy and limited by challenges in tracking cloud advection and satellite imager resolution constraints (Sieglaff et al. 2011).

Recent advances in brightness motion, or optical flow (OF; Horn and Schunck 1981) retrieval techniques, offer a promising new approach to tracking cloud-top evolution in a semi-Lagrangian framework at a near-pixel level (Apke et al. 2020). Such techniques are enabled for most cloud and water vapor drift motions by the enhanced resolutions of current generation of geostationary satellite imagers, such as the Geostationary Operational Environmental Satellite

(GOES)-R series Advanced Baseline Imager (ABI; Schmit et al. 2017). By following the motion of individual cloud pixels over time, hence "dense OF" (DOF), DOF-based CTC retrievals from ABI can provide unprecedented time-trends without common sensitivities related to cloud merging and splitting with previous tracking systems. Since CTC should directly correspond to initial updraft intensity, two questions arise:

1. How does DOF-based CTC relate to ambient instability?
2. How does DOF-based CTC relate to the timing of significant and severe deep convection?

Answering these questions is critical for improving short-term forecasting and nowcasting capabilities. By linking CTC (a satellite-observed signal of vertical cloud growth) to ambient instability, Research Question (1) helps explore whether satellite-derived CTC can serve as a real-time proxy for ambient environmental thermodynamics. This linkage is especially valuable in the early stages of storm development, when radar may not yet detect precipitation. If a strong positive correlation exists, forecasters could use CTC as a more immediate and spatially continuous indicator of how and where storms are likely to intensify (especially when considering the dwindling rawinsonde observations, which typically provide vertical profile information). This research hypothesizes if CTC is correlated to the ambient instability (as is the case for updraft strength), we should be able to observe two relationships: 1) CTC should increase with altitude as DC grows from the Level of Free Convection (LFC) to the Equilibrium Level (EL), and rapidly diminish after a parcel reaches the EL, and 2) The peak CTC should be higher for storms that exist in environments with stronger ambient instability.

Likewise, DOF-based CTC offers a way to observe the rapid vertical development of clouds at an unprecedented fidelity in near real-time. If, like previous research, DOF-based CTC

consistently precedes severe DC, it could be used to extend lead times for severe weather alerts, especially in data-sparse regions or during the early, non-precipitating stages of convection. However, if such lead-times are long (i.e. > 15 min), end-users must decide how to effectively warn with such information without issuing too early (especially in strong storm motions). As CTC, when effectively tracked, is already known to precede severe weather occurrences (Mecikalski et al. 2021), Research Question (2) is designed to explore the timing of such severe weather occurrences and whether relationships exist between timing and the CTC strength. The research also hypothesizes that if DOF-based CTC is related to initial DC updraft strength, then strong CTC events will have a shorter lead time to significant and severe returns on radar than weaker CTC events.

To address these science questions, this study leverages high-resolution satellite data from the GOES-16 ABI, radar observations from an advanced mosaic system, and thermodynamic profiles from a high-resolution NWP model. DC CTC features are segmented and tracked using an objective framework and matched with radar-based storm tracks to assess timing and severity. By automating the detection and tracking process, the methodology ensures consistency, scalability, and objectivity in the selection of case studies, while also allowing for detailed examination of individual events.

This research is organized as follows: Chapter 2 provides a review of the scientific background, including prior research on CTC, its relationship to updraft strength and storm severity, and the evolution of OF retrieval techniques in satellite meteorology. Chapter 3 outlines the data sources, CTC retrieval methods, and the automated tracking and analysis framework used in this study. Chapter 4 presents the results, including statistical analyses and case studies

that address the two core research questions. Finally, Chapter 5 summarizes the key findings, discusses limitations, and proposes directions for future research.

2. BACKGROUND: CLOUD TOP COOLING AND OPTICAL FLOW

2.1 Cloud Top Cooling

2.1.1 Introduction to CTC

CTC refers to the rapid decrease in temperature at the uppermost layer of a cloud detected by the satellite. This cooling is directly related to the vertical motion of the cloud-top, where rising air parcels cool adiabatically as they ascend to lower pressures (Petty 2008). As such, CTC serves as a proxy for updraft strength (which is difficult to measure with conventional ground-based observational systems and is a critical early indicator of DC development). Rapid CTC is often associated with the intensification of thunderstorms and the potential for severe weather (Mecikalski et al. 2021), making it a valuable parameter in short-term weather forecasting, or nowcasting, which focuses on the 0–3 hour timeframe. In this context, the timing of CTC onset is especially important: identifying when rapid cooling begins can provide forecasters with crucial lead time to anticipate storm development before it becomes evident in radar or surface observations. This temporal advantage is vital for issuing timely warnings and improving public safety during rapidly evolving severe weather events.

2.1.2 Cloud Top Cooling Relationships to Updraft Growth and Environmental Properties

The connections of CTC to updraft growth can be traced back to the pioneering work of Adler and Fenn (1979), who utilized early geostationary satellite imagery to distinguish between ordinary and severe thunderstorms. With IR brightness temperature data from legacy GOES satellites, they monitored storm evolution across the Great Plains by subjectively analyzing sequential images for changes in cloud-top temperature and anvil expansion and noted greater values for severe and non-severe thunderstorms. Despite the coarse spatial resolution (~7 km),

limited temporal refresh, and poor navigational capabilities of early GOES sensors, their work enabled future advancements in satellite-based storm monitoring. In parallel, by using dual geostationary satellite views, Mack et al. (1983) demonstrated how geometric triangulation could estimate cloud-top heights and track their ascent over time. This method offered a direct way to observe vertical motion, a key indicator of updraft strength. However, operational use was limited by technical challenges, including satellite alignment, parallax correction, and cloud feature matching (Mack et al. 1983; Hasler et al. 1991; Wylie et al. 1998), leaving most future research to focus on CTC instead.

The relationship between satellite-derived CTC and environmental thermodynamic properties has been a focal point of recent research, both for creating objective retrievals of instability in the absence of weather balloon upper air soundings and for attempting to identify early signals of convective inhibition. In the absence of clouds, satellite-based retrievals from passive hyperspectral infrared and microwave imagers such as the NOAA Unique Combined Atmospheric Processing System (NUCAPS) have been developed to address these gaps by providing global vertical profiles of temperature and moisture (Feltz et al. 2017). While NUCAPS represents a step forward in environmental characterization, it still faces limitations in spatial resolution, latency, and accuracy in cloudy or convectively active regions. To account for these cloudy scenes, Mecikalski et al. (2016) subjectively tracked 1-minute Super Rapid Scan Operations for GOES-R (SRSOR) data to examine cumulus cloud updrafts and their vertical development in relation to environmental buoyancy profiles. Their analysis revealed that updraft acceleration, as inferred from cloud-top brightness temperature trends, was correlated with the amount of convective available potential energy (CAPE) realized during cloud growth. Notably, these relationships were observed despite inherent limitations in the study, such as coarse spatial

resolution, low sample size (due to time-consuming subjective collection), and the inability to directly observe in-cloud processes. The study implies that the most rapid cloud growth typically occurred above the 0°C isotherm, coinciding with cloud-top glaciation, suggesting a strong link between latent heat release and enhanced vertical motion.

Beyond initiation, CTC has also been linked to storm severity. Sieglaff et al. (2014) and and Hartung et al. (2013) demonstrated that stronger and more persistent CTC signals were often associated with storms that later produced severe weather, including large hail and damaging winds. These studies showed that rapid and sustained cooling rates could serve as early indicators of robust updrafts conducive to severe weather. Mecikalski et al. (2021) further expanded on this by integrating CTC metrics into probabilistic random-forest-based nowcasting frameworks, showing that CTC trends along with satellite motion characteristics, such as cloud-top speed, could enhance the prediction of storm intensity when combined with radar and lightning data.

2.1.3 Automated Retrievals of Cloud Top Cooling

Efforts to automate the detection of CI through satellite-based CTC retrievals have advanced significantly over the past two decades. These methods aim to identify early signals of vertical cloud development by monitoring trends in IR brightness temperatures, which often precede the establishment of rain/hail hydrometeors and thus radar-detectable convection. The foundational work by Roberts and Rutledge (2002) demonstrated that rapid cooling of cloud tops to subfreezing temperatures could serve as a precursor to convective storm development. They objectively retrieved motions and tracked convection using, 20 km^2 windows. This domain size was chosen because it is small enough to isolate individual convective elements, yet large enough to account for cloud and boundary motion over a typical 4-hour afternoon convection

period. Their analysis showed that satellite-derived cooling rates, when combined with radar observations of boundary layer convergence features, provided valuable lead time, up to 30 minutes, before the appearance of significant radar reflectivity. This research provided a framework for integrating disparate satellite and radar data into a single automated nowcasting system.

Building on these insights, Mecikalski and Bedka (2006) developed the Satellite Convection Analysis and Tracking Algorithm (SatCast), one of the first attempts to automate CTC detection without the assistance of radar (thereby expanding the viable spatial domain). SatCast employed segmented cloud tracking and relatively sparse (when compared to current tracking capabilities) mesoscale Atmospheric Motion Vectors (AMVs; Bedka and Mecikalski 2005) to monitor cloud properties in visible and infrared channels from GOES satellites. The algorithm evaluated spectral trends beyond CTC, including brightness temperature and multispectral differences from water-vapor bands, and used logistic regression to estimate the probability of CI. While SatCast demonstrated skill in forecasting isolated convection up to 45 minutes in advance, its performance was constrained by limitations in satellite resolution, AMV scarcity, and contamination from cirrus clouds, which often obscured signals from lower-level cloud development. Furthermore, no attempt was made to quantify the timing of severe weather occurrence after high-probability CI objects were detected, limiting the product's utility in operational settings.

Subsequent advancements were made with the University of Wisconsin's CTC algorithm (UW-CTC; Sieglaff et al. 2011). This method utilized a boxcar-averaging technique to compute mean brightness temperatures within small grid boxes and tracked their temporal evolution to detect cooling, eliminating dependence on AMVs and segmentation. Operating continuously in

both day and night conditions, the algorithm incorporated several filters to reduce false signals from horizontal cloud motion and other non-convective processes. Validation against cloud-to-ground lightning initiation events revealed that the algorithm performed best in clear-sky environments and along sharp boundaries, but its effectiveness diminished in the presence of cirrus shields, existing anvils, and fast-moving clouds. The algorithm's probability of detection (POD) was modest, with nearly half of CI events missed and a false alarm rate (FAR) of approximately 25%. Furthermore, the temporal resolution of the GOES-13 satellite imager (15 min for full-disk) often resulted in sub-zero-minute lead times, limiting the algorithm's operational utility.

In response to operational forecaster feedback from demonstrations at numerous testbeds, the UW-CTC algorithm later evolved into the ProbSevere framework (Cintineo et al. 2018). ProbSevere tracks cloud objects using a multi-scale objective segmentation framework like SatCast to combine satellite, radar, lightning, and NWP data to assess the probability of severe weather events within the next hour, output as simple shapefiles to be overlaid with radar datasets (Cintineo et al. 2014, 2020). The inclusion of CTC outputs coupled with the stability of ground-based radar observations improved the system's ability to detect early convective signals and extended lead times for severe weather alerts. This integration of disparate datasets into a single, simple to use framework marked a significant step toward use of satellite-based CI detection within operations. The dependence on segmented tracking, however, introduces problems when cloud objects merge or split, a problem that persists in the product today (Cintineo et al. 2020).

Building on the success of ProbSevere, additional deep-learning-based nowcasting tools have been developed to further improve CI detection. One such tool is LightningCast (Cintineo

et al. 2022), a convolutional neural network trained on GOES-16 ABI imagery and Geostationary Lightning Mapper data. LightningCast provides probabilistic guidance for lightning occurrence in the next 60 minutes, using only satellite imagery as input. It has demonstrated skill in predicting both developing and advecting storms, often providing >20 min lead time to lightning initiation. Its ability to operate independently of radar makes it particularly valuable in regions with limited radar coverage. Another similar advancement is ThunderCast (Ortland et al. 2023), a deep learning model designed to nowcast thunderstorm occurrence using GOES-16 ABI data to predict Multi-Radar Multi-Sector (MRMS) radar reflectivity occurrence at the −10 °C isotherm in the next hour. It has shown skill in a variety of convective environments, including mesoscale convective vortices, sea-breeze convection, and monsoonal storms. ThunderCast is especially promising for its ability to provide both lead time and timing of DC initiation in radar-limited areas, though research is still ongoing to identify critical signals in input datasets that give the deep learning models information on where to make predictions. Furthermore, neither model yet engages with time-based information, which can be extracted with the help of novel DOF-based tools.

2.2 Optical Flow

AMVs have long served as a critical tool in Earth observing systems, offering estimates of horizontal wind fields even in data-sparse regions by tracking the apparent motion of clouds and water vapor features in satellite imagery sequences. Traditionally, AMVs were derived using patch-matching (PM) techniques, which identify and track small image regions (or "targets") in the imagery across time. These methods, while foundational, rely on assumptions of traceability, including brightness constancy and neighborhood consistency within the target (e.g., a 15x15

pixel box ~56 km^2), which often break down in complex atmospheric scenes, particularly in low-texture or multilayer cloud environments (Apke et al. 2022).

The underlying principle of AMV derivation is rooted in OF retrieval, a concept introduced by Horn and Schunck (1981), which quantifies the apparent motion of brightness patterns in image sequences. Over the past four decades, OF retrieval techniques have evolved significantly, driven by advances in computer vision and computational power (Fortun et al. 2015). These developments have enabled more sophisticated techniques, known as variational optical flow (VOF), which estimates motion fields by minimizing energy functions even in difficult-to-track regions such as those with low texture, strong deformation, transparencies, illumination changes, and motion discontinuities.

Such advancements have significant implications for both research and operational forecasting. Improved motion tracking enables better characterization of cloud-top dynamics, including the detection of outflow boundaries, CI, and storm intensification (Apke et al. 2018, 2020; Apke and Mecikalski 2021). As satellite capabilities continue to evolve, the fusion of novel OF retrieval techniques with high-resolution geostationary imagery holds promise for enhancing severe weather nowcasting and NWP. Recent work by Vandal et al. (2022) further supports this trajectory by introducing WindFlow, a deep learning-based OF retrieval system trained on high-resolution numerical simulations and transferred to satellite imagery. Their results demonstrate that machine learning-based OF can produce dense, accurate wind fields with low bias and strong agreement with rawinsonde observations, offering a scalable and efficient alternative to traditional AMV techniques that function on water vapor imagery.

While recent advances in OF techniques have significantly improved the accuracy and spatial coverage of cloud-top AMVs, much of the focus has been on validating motion retrievals or enhancing flow field resolution (Ouyed et al. 2021; Apke et al. 2022; Yanovsky et al. 2024). However, the potential of these techniques extends beyond motion estimation alone. With the advent of high-temporal-resolution satellite imagery, such as 1-minute scans from the GOES-R series, OF can now be used to derive not only motion but also time-evolving properties, such as CTC. This capability opens new avenues for diagnosing the life cycle of DC with unprecedented temporal precision and spatial accuracy. VOF tracking enables better characterization of complex cloud-top flows without the need for objective image segmentation (Stettner et al. 2019; Apke et al. 2020). When used to compute CTC, it is likely that relationships to DC environments and severity subjectively identified with manual tracking would be objectively resolvable. This is particularly valuable for identifying rapidly intensifying convective cells in complex DC environments, which are often precursors to severe weather events. The current research investigates how this novel DOF-based CTC product can provide early and reliable indicators of storm initiation, environments, growth, and severity.

3 RESEARCH METHODOLOGY

3.1 Data Sources

This study makes extensive use of both radar and satellite data. Satellite observations were obtained from the GOES-16 (GOES-East) ABI, parked at 75.2° W, specifically utilizing its 10.3 μm infrared channel (Schmit et al. 2017). The analysis focused on data from the mesoscale sectors, which offer high temporal (1–min cadence) and spatial (~2 km nominal at nadir) resolution. NOAA's NESDIS Operations Center dynamically positions these mesoscale sectors to monitor regions of interest such as severe weather outbreaks, wildfires, and hurricanes (Line et al. 2015). During periods of quiescent weather, the sectors default to two locations and may also be repositioned to support rocket launches or field research campaigns. The automated analysis focused on a three-month period (April-June) during the peak of the 2024 convective season. Throughout this convective season, cases were found in mesosectors positioned in the central United States, including the Deep South, Great Plains and lower Midwest (Figure 1). During periods of calm weather, the mesosectors are in two default locations, one in the Northeast and Mid-Atlantic (Meso-1; centered at 38.5° N, 75° W) and one in the lower Midwest to Southeast (Meso-2; centered at 37° N, 86.5° W). These two locations, especially Meso-2's default location, have been used by the automated algorithm on multiple days for the 2024 convective season (hotter colors on Figure 1). It is important to note that on certain days, mesoscale sectors were positioned outside the CONUS domain, primarily in response to tropical systems or data requests from NOAA international partners.

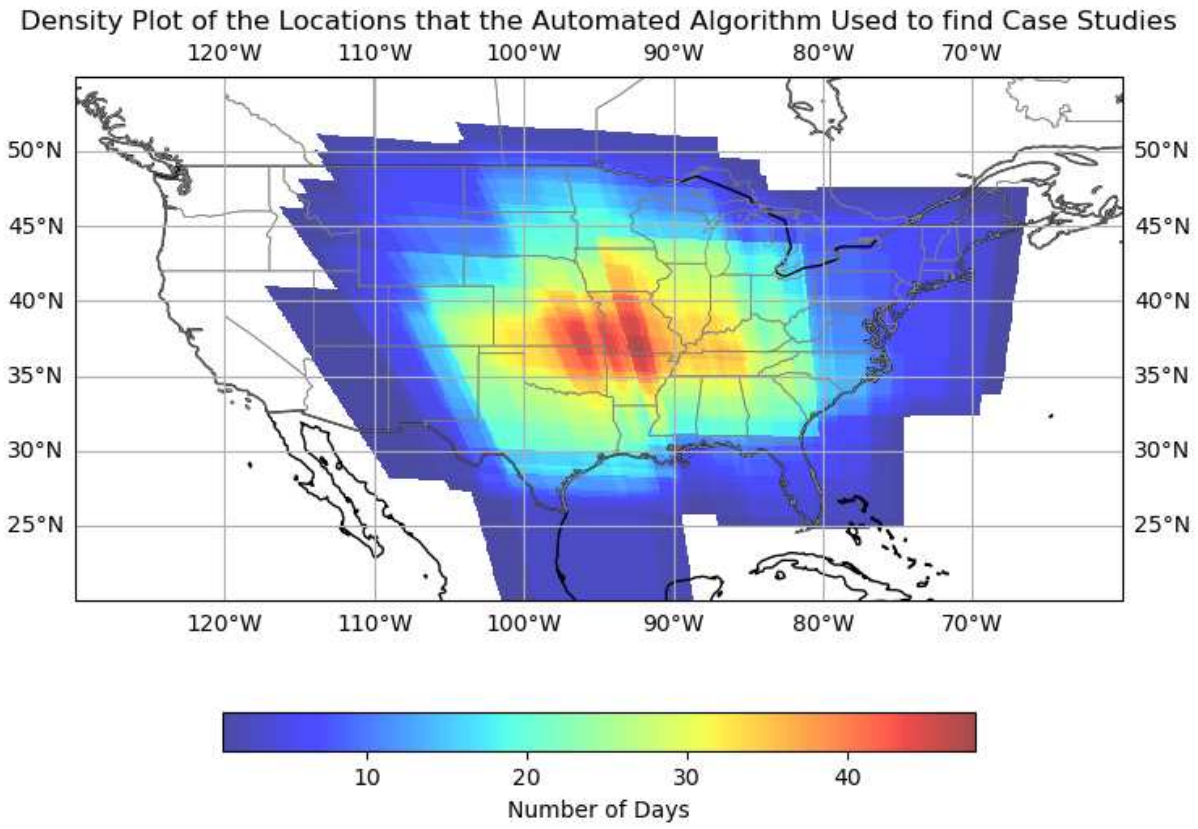

Figure 1: Density plot of the mesosector locations on GOES-16 in which the automated algorithm found cases.

Radar data were sourced from the MRMS operational dataset (Smith et al. 2016). MRMS integrates data from over 180 radars, surface observations, satellite, lightning, and NWP models into a unified, high-resolution 3D grid. This composite provides a more complete and seamless depiction of precipitation than any single radar can offer alone, at a 2–min cadence and 0.01° x 0.01° resolution. The MRMS dataset applies quality control to mitigate/remove non-meteorological echoes (e.g., ground clutter, biological returns, sun spikes) and meteorological artifacts (e.g., bright banding, three-body scatter spikes), ensuring cleaner and more reliable data for research (Smith et al. 2016). In this research, three products of MRMS were used: 1) Reflectivity values were extracted at the -10 °C isotherm, 2) Hail size estimates were derived using the Maximum Estimated Size of Hail (MESH) algorithm, and 3) A quality index filter,

from the Radar Quality Index (RQI), was used to remove areas of the United States with poor radar coverage, due to outages, terrain, or lack of nearby radars where MESH values could not be accurately calculated across the column.

Additionally, atmospheric thermodynamics, including instability, were assessed using the NOAA Rapid Refresh (RAP) model. RAP provides hourly analysis field updates, with a horizontal resolution of 13 km and 50+ vertical levels from the surface to 100 hPa (Benjamin et al. 2016). In this thesis, temperature and dewpoint profiles were retrieved to compute the Most Unstable Convective Available Potential Energy (MUCAPE) for each case study (see Section 3.4 for further details). As an operational NOAA model, RAP is well-documented and freely available, making it a valuable resource for retrospective research. The RAP is used here versus NOAA's finer-spatial resolution High Resolution Rapid Refresh (HRRR) model to be consistent with similar empirical research (e.g. Cintineo et al. 2014) and such that mesoscale convection environmental and thermodynamic characteristics are captured.

3.2 CTC Retrieval

The Optical Flow Code for Tracking, AMV, and Nowcasting Experiments (OCTANE; see Apke et. al 2022) was used on the GOES-16 ABI mesoscale sector 10.3 μm infrared channel to render the OF field. The brightness temperature change following the storm motion is what is defined here as the CTC. OCTANE uses a variational penalty function minimization technique, which renders accurate, dense (every image pixel) motions in satellite imagery sequences following decades of advancements by the computer vision community (Apke et al. 2022). Unlike traditional AMV computations, such as Velden et al. (2005), which use least-squares or cross-correlation-based PM to track discrete, high-contrast features and fail on low-texture and multilayer clouds, OCTANE uses two input images and a first-guess motion field (typically a

field of stationary motions) to iteratively solve for the actual motion field via minimizing a specially designed penalty function with gradient descent methods. Variational penalties *E* that are minimized assume the actual OF $\boldsymbol{u}$ allows a set of mathematical rules designed to mimic human vision interpretation. The penalties are minimized at every image pixel defined as $\boldsymbol{\Omega}$. This method assumes that the actual OF field tracks consistent image brightness and brightness gradients and is realistically smooth (Zimmer et al. 2011) posed as:

$$E(\boldsymbol{u}) = \sum_{i,j\in\Omega} [\rho_d(BC_{i,j}) + \lambda\rho_g(GC_{i,j}) + \alpha\rho_s(SC_{i,j})] \quad (1)$$

where the brightness (BC), brightness gradient (GC), and smoothness (SC) constraints are encapsulated in robust functions $\rho_d, \rho_g,$ and $\rho_s,$ to preserve motion discontinuities in the retrieval. λ and α are tunable constants that control the relative strength of each penalty. VOF methods like this one are demonstrated to render accurate motions even in difficult-to-track scenes, such as those with deformations, motion discontinuities, transparent motions, illumination changes, and low texture (Fortun et al. 2015). Minimization of (1) to solve for $\boldsymbol{u}$ is enabled by smaller frame-to-frame displacements (via assumptions made in the linearization of the constraints) and fewer occurrences of growth or decay of clouds, which for DC requires 1 min refresh imagery (Apke et al. 2016, 2018; Apke and Mecikalski 2021). In this experiment, CTC is quantified in units of Kelvin per five minutes (K 5 min^{-1}), a resolution made possible by the rapid 1 min scan intervals of GOES-R series satellites. This temporal granularity allows for more accurate detection of convective growth at finer scales (e.g. see Mecikalski et al. 2016), which can be

compared to earlier studies using heritage GOES imagery, which typically offered only three images over a 15-minute period.

The VOF method applied in this study to calculate CTC enables a detailed and accurate representation of atmospheric motion, allowing for precise pixel tracking and temperature difference calculations. This approach is particularly powerful when leveraged with the high spatial and temporal resolution data provided by the GOES mesosectors. CTC computation with VOF methods is, however, subject to some tracking error (winds in Apke et al. 2022, for example, were typically accurate to only within 4-6 m s^{-1}), which, if left unchecked, can produce large artifacts near strong infrared brightness temperature gradients (e.g. the edges of mature DC; Figure 2a). Such artifacts are reduced with a special minimum filter applied to the 10.3 μm image at time t – 5 min (I_{t-5}) that ensures the returned temperature difference applies only to changes in regional minima (as a human commonly interprets the imagery; Figure 2b). For each pixel in I_{t-5}, the filter searches for the coldest brightness temperature within 2 pixels of the pixel center, and any colder pixels within 4 pixels that are both a) not moving away from the pixel center (as determined by the VOF output), and b) not separated from the center pixel by a warm brightness temperature canyon. Part b) is determined using a "ray tracing" check between the candidate minimum and the center pixel to ensure there is no significant warm region separating them, which helps to avoid over-filtering when convection initiates near higher, colder clouds.

Integrated CTC is introduced as an enhancement to traditional CTC metrics. In addition to identifying instantaneous CTC values, this study computes a running 3–min sum of the CTC track and records the maximum value found within this window. This integrated approach allows for differentiation between storms that exhibit sustained, strong CTC signals over several

minutes—indicative of longer-lived, potentially more intense convective systems—and those that only show brief, isolated peaks in CTC.

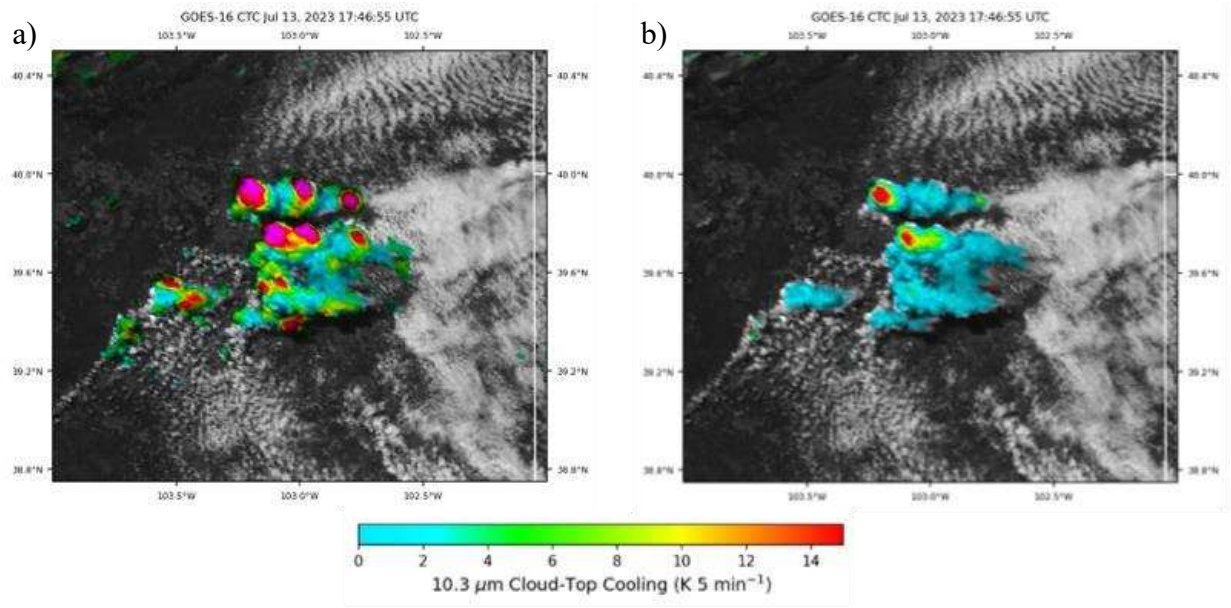

Figure 2: DOF-CTC product (colors) blended with the GOES-16 0.64 µm reflectance (brightness) over a CI event over Eastern Colorado at 17:46 UTC on 13 July 2023 where hotter colors indicate stronger CTC values, with cyan color indicating clouds <0° C, shown with a) the product before and b) after IR Minimum Filter was applied.

3.3 Segmentation and Tracking of Deep Convection

The workflow here is an automated analysis process for a full day of GOES-16 mesoscale sector data (Figure 3). A broad overview of this workflow for one days' worth of cases starts with using data from MRMS and CTC to identify features and link them together to create storm tracks. These MRMS and CTC storm tracks are then matched to create a case study, and this case study will subsequently be used to understand the ambient instability and CTC strength, along with the timing of CTC and subsequent radar returns.

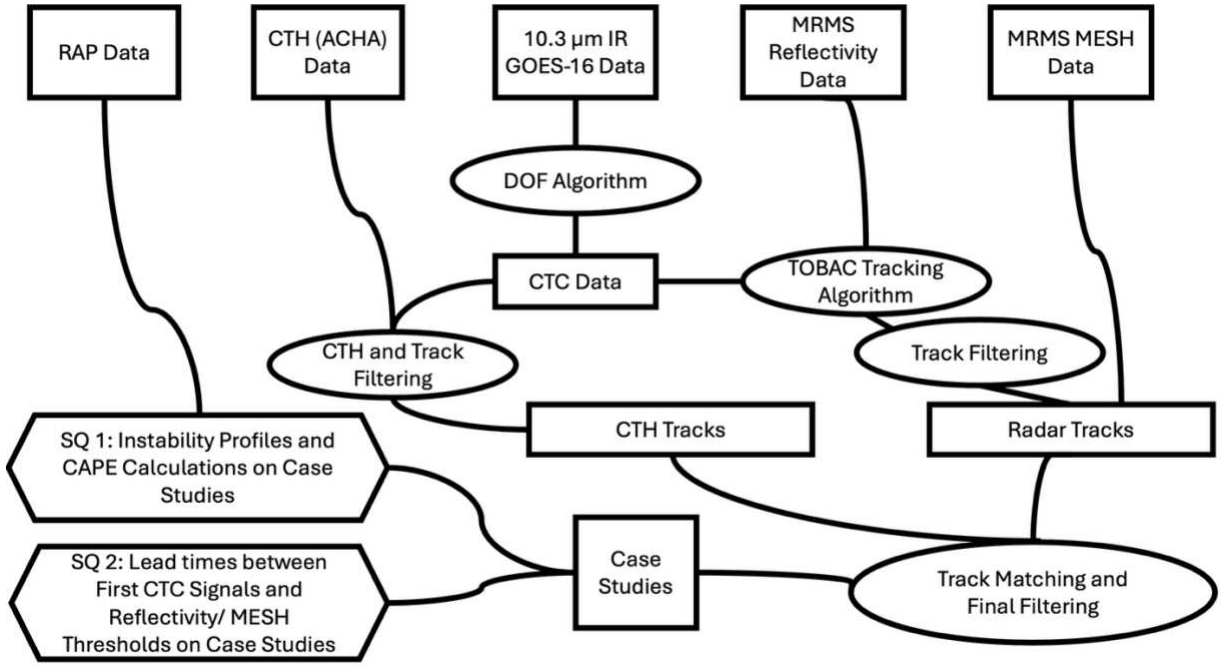

Figure 3: Flowchart illustrating the automation process for analyzing a full day of GOES-16 mesoscale sector scenes.

The workflow includes automated tracking using the Tracking and Object-Based Analysis of Clouds (TOBAC) algorithm (Sokolowsky et al. 2024), followed by backtracking and filtering to identify relevant case studies for subsequent analysis. TOBAC is a flexible, Python-based framework designed for identifying, segmenting, and tracking meteorological features in gridded datasets, including 2D satellite imagery, 3D model output, and radar composites. Unlike traditional pixel-based or centroid-tracking methods, TOBAC enables object-based detection using user-defined thresholds for feature intensity (e.g., maxima or minima) and spatial extent (e.g., pixel count), which is particularly advantageous for isolating convective features that meet criteria for severity and significant vertical development. TOBAC was selected over other tracking frameworks such as W2segmotion or TITAN due to its modular design, adaptability across data types, and its ability to incorporate physically meaningful constraints like maximum displacement and feature memory (Dixon and Wiener 1993; Lakshmanan and Smith 2010). While W2segmotion is optimized for real-time operational use and excels in tracking well-

defined radar echoes, it is less flexible for research applications involving multi-source datasets like CTC fields and requires significant postprocessing to manage merging and splitting cells in operational settings (Cintineo et al. 2020).

TOBAC's use of the TrackPy backend allows for probabilistic linking of features across time steps, accounting for velocity, displacement, and feature evolution in a manner which follows human interpretation. For this study, TOBAC was applied separately to radar reflectivity and CTC datasets. The feature detection, segmentation, and tracking parameters used for each dataset are summarized in Tables 1 and 2. These settings were adapted from prior research using TOBAC on MRMS reflectivity data (Scarino et al. 2023) and from default configurations provided in TOBAC's example open-source repositories (Sokolowsky et al. 2024). Additionally, parameter tuning was performed heuristically by visually inspecting the tracking output across several convective cases to ensure that the algorithm captured the full lifecycle of convective cells without over-segmenting or prematurely terminating tracks. This iterative tuning process was essential to balance sensitivity and specificity in both radar and satellite-derived fields, ensuring robust and interpretable tracking results

Table 1: Settings used for TOBAC MRMS radar reflectivity tracking**.**

Feature Setting	**Threshold used for detection**
Position Threshold	extreme
Sigma Threshold	1
N Min Threshold	15
Minimum Distance between features	0.125 degrees
Target	Maximum
Thresholds for Features	Every value from 35-70 dBZ
Segmentation Setting	**Threshold used for Segmentation Output**
Method	Watershed
Target	Maximum
2D Watershed Segmentation Thresholds	35 dBZ
Track Setting	**Threshold used for track output**
V Max	50
Stubs	2
Order	1
Adaptive stop	0.2
Adaptive step	0.95
Subnetwork Size	100
Method Linking	Predict
Memory	0 min

Table 2: Settings used for TOBAC CTC tracking.

Feature Setting	**Threshold used for detection**
Position Threshold	extreme
Sigma Threshold	1
N Min Threshold	4
Minimum Distance between features	0
Target	Maximum
Thresholds for Features	2,5,10,12,15 (K 5 min^{-1})
Segmentation Setting	**Threshold used for Segmentation Output**
Method	Watershed
Target	Maximum
Track Setting	**Threshold used for track output**
V Max	100
Stubs	2
Order	1
Adaptive stop	0.2
Adaptive step	0.95
Subnetwork Size	10
Method Linking	Predict
Memory	5 min

The VOF-based CTC computation is still susceptible to errors related to thin overcast cirrus moving over developing cumulus. To mitigate such contamination, the Cloud Top Height (CTH) algorithm was applied as a filter to the CTC output. The CTH algorithm, formally known as the Algorithm Working Group Cloud Height Algorithm (ACHA), estimates cloud-top height, pressure, and temperature using a one-dimensional variational (1D-Var) optimal estimation approach (Heidinger et al. 2020). It combines radiances from multiple infrared channels—typically centered around 8.5 µm, 10.7 µm, and 12.0 µm—to retrieve cloud-top properties across both day and night conditions. By leveraging ancillary data from NWP models, ACHA translates retrieved cloud-top temperatures into physical heights and pressures. This method is particularly

effective at identifying and characterizing high-level clouds, such as cirrus, which can obscure or distort signals from underlying convective development. ACHA is used here to remove any candidate CTC tracks from further analysis if they are deemed to be covered by a higher, thin cirrus layer. Once TOBAC was confirmed to successfully identify and track features, additional filtering was applied to refine the dataset (Table 3). Filtering heuristics were decided to limit case studies to the initial updraft growth. Filtering CTC output with ACHA-derived CTH ensures that only pixels associated with genuine vertical cloud growth are retained, thereby improving the reliability of CI diagnostics. Filtering based on RQI also allows for the removal of tracks in which MESH values cannot be able to be accurately calculated across the column.

Table 3: Track filtering used to find case studies.

Track Filter	Comments
CTC	0.25°x 0.25° area around track has clouds that are < 7 km in height
	Tracks need to be >= 7 min in time
	Tracks need to have a RQI >= 50%
Radar Reflectivity	Tracks need to be >=20 min in time

A linear backtracking procedure was implemented to associate satellite-based CTC features with radar-based storm tracks. This step required an adjustment for parallax-induced shift of 6 km to shift the radar tracks onto the satellite grid, accounting for the satellite viewing geometry and Earth's curvature. The radar tracks were then interpolated to a 1 min cadence to match the satellite temporal resolution. The backtracking algorithm computed the mean displacement vector over its first five minutes. Using this motion estimate, the algorithm calculated backward both in location on Earth and satellite imagery coordinates up to 45 min prior to the first radar detection. This enabled the identification of precursor CTC signals associated with developing DC. CTC and radar tracks were matched using a temporal and

spatial overlap where track centroids were within 0.25° (longitude and latitude) or ~25 km. In cases where multiple radar tracks intersected a single CTC track, the temporally longest radar track was selected. Each matched pair was treated as a distinct case study used to address the primary research questions detailed below.

3.4 CTC Relationships to Atmospheric Instability

Ambient instability was assessed using RAP model soundings, extracted at the grid point nearest to the earliest feature in each CTC track. For each case, the previous three hours of RAP analyses were retrieved, and the most unstable parcel profile was used for further calculations. Temporal composites like this are done to mitigate issues related to boundary timing that are common in NWP models (e.g. see Cintineo et al. 2022). The most unstable sounding from the composite was used to estimate expected CTC growth for individual DC case studies,. CAPE was then calculated in this sounding using the trapezoidal rule at 25 mb intervals from the LFC to the EL using the temperature and dewpoint vertical profiles. CAPE was then integrated in 25 hPa increments to construct a vertical instability profile (Figure 4a). From these CAPE values, vertical velocities were inferred using Eq (2), a simplified relationship between CAPE and the

$$\sqrt{2\mathrm{CAPE}} = \omega_{\max} \tag{2}$$

maximum vertical velocity (ω max) within a thunderstorm updraft. These vertical velocities were subsequently converted to expected CTC values using Eq. (3)

$$\frac{meters}{sec} * \frac{60\ sec}{1\ min} * \frac{5\ min}{5\ min} = \frac{meters}{5min} * \frac{Avg.\ K}{dh\ (meters)} = \frac{Avg.K}{5\ min} \tag{3}$$

This maximum vertical velocity (ω max) in m s^{-1} is converted to an expected maximum CTC, K 5 min^{-1}. *Avg. K* in (3) is the temperature at the level used to compute CAPE, and *dh* is the height at that layer, from the geopotential at that layer. The mean temperature within each 50 mb layer was assumed to represent the brightness temperature observed by the GOES-16 10.3 μm channel.

These expected CTC profiles were then compared to observed CTC values to evaluate how closely CTC retrieved via ABI and DOF aligns with predictions made by idealized thermodynamic relationships inferred with parcel theory (Figure 4b). Additionally, the maximum observed CTC was compared to the maximum MUCAPE from the RAP profile to assess the relationship between instability and CTC strength. In previous CTC experiments with heritage GOES satellites, past research suggests that the relationship between CTC events and CAPE is linear and proportional to one another. This thesis builds on this previous work by taking the CTC values at a one-minute cadence objectively and tracking growth for a large sample size.

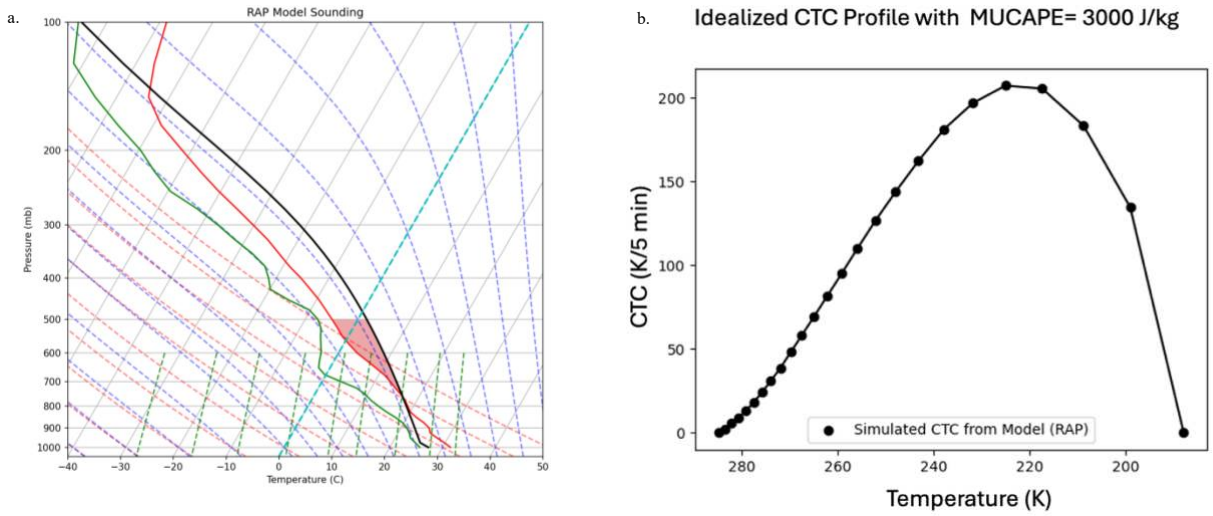

Figure 4: a) Example case study from 1 Aug 2024 of a RAP model sounding with CAPE calculated (red shade) at the 500 hPa using the trapezoidal rule and a total MUCAPE = 3000 J kg^{-1}, shown with b) the example case study estimated CTC growth curves (CTC vs temperature) from the RAP model Sounding.

3.5 CTC and Severe Hail Timing

The second component of the analysis focused on identifying any timing relationship between CTC signals and storm initiation and severity indicators. For an objective definition of significant DC initiation, this research uses a 35 dBZ at -10 °C that covers a defined area, which commonly correlates to the initial occurrence of lightning and strong precipitation at the surface (e.g. Mecikalski and Bedka 2006). For determining storm severity, this research uses the MRMS MESH product (e.g. when MESH exceeds 1" diameter). While MESH is only an approximation of hail location and size, it is preferable to ground-based storm reports which fail to capture the event size and exact timing (e.g. Mecikalski et al. 2021).

Table 4 outlines the specific threshold values used here. For each case, the lead time was calculated as the time difference between the CTC threshold crossing and the corresponding threshold crossing in the radar reflectivity or MESH dataset. These lead times were then compared to the maximum observed CTC in each case. Because only a subset of cases met the

MESH-based severity criteria, the sample size for this analysis in the following section is expected to be smaller than that used for Section 3.4.

Table 4: Thresholds used to determine lead times between CTC and Significant/Severe DC

Data Source (units)	Threshold Value
CTC (K/5 minutes)	First instance of >=12 K/5 minutes
Reflectivity at constant -10 °C isotherm (dBZ) (Significant DC)	First instance of >= 35 dBZ and size >= 49 km^2
MESH (inches) (Severe DC)	First instance of >= 1 inch

4. RESULTS AND DISCUSSION

4.1 Database Characteristics

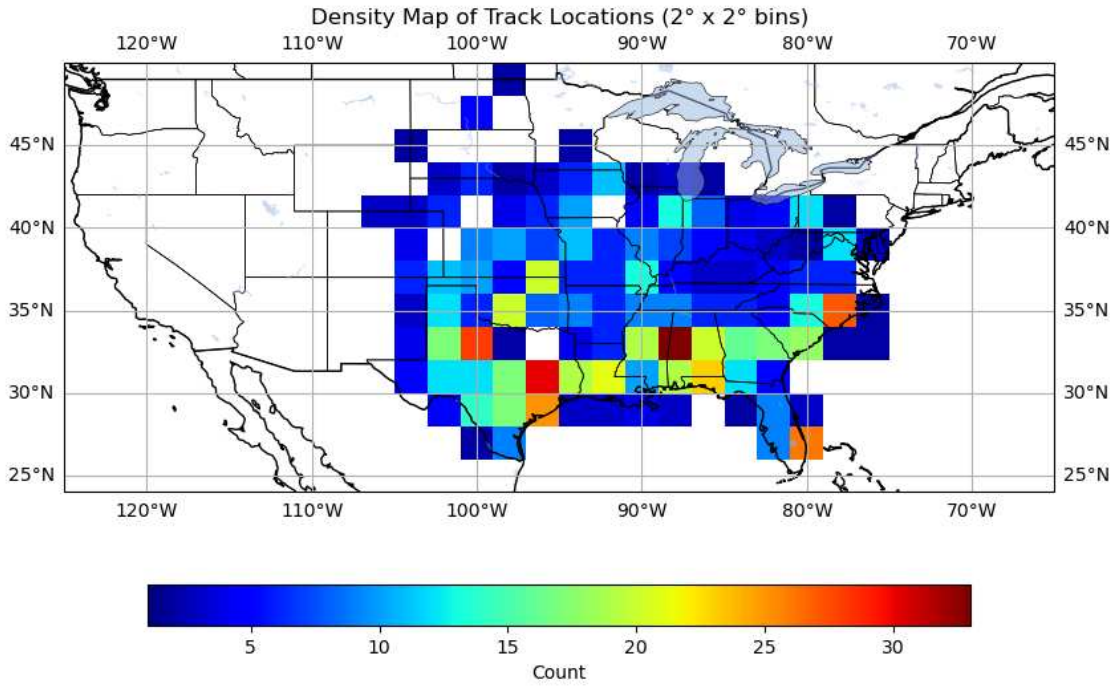

Figure 5: Density plot of the 1,063 automated case study tracks, that are in a 2° x 2° bin.

In total, 1,063 CI cases were identified for the months of April, May, and June of 2024. Due to the dynamic positioning of GOES mesosectors by the NOAA-NESDIS Operations Center, there were ~25 days with mesosector scenes where no cases were retrieved. This absence was primarily due to either (1) lack of radar coverage within the mesosector (e.g., scenes located outside the CONUS, such as over tropical systems or research campaigns) or (2) the absence of convective features in the CTC or radar datasets. The latter typically occurred when mesosectors were allocated for non-convective monitoring, such as wildfires, or were positioned over regions

experiencing calm, clear weather (e.g., the default locations over the lower Midwest and Northeast).

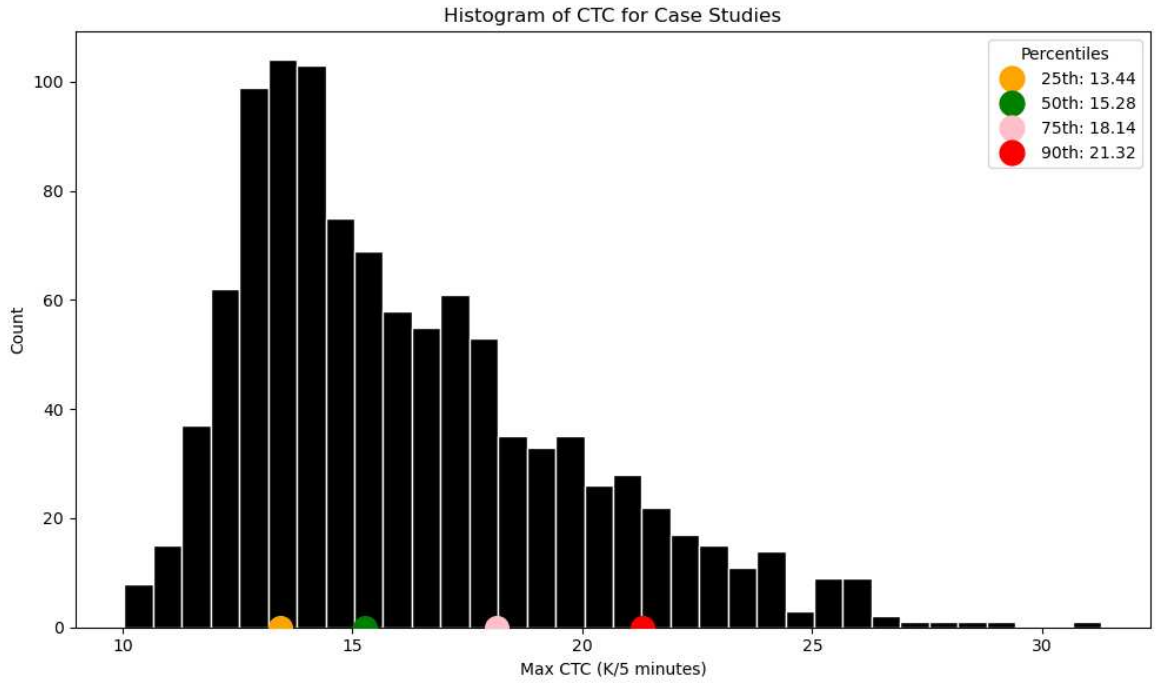

Figure 6: Histogram of the 1,063 cases, based on maximum CTC strength. The x-axis represents Maximum CTC in K 5 min^{-1}, while the y-axis indicates the number of cases within each CTC bin.

In this study, 81 unique GOES-16 mesoscale sector scenes were analyzed in this study. Density maps of storm track locations (Figure 5) revealed a strong spatial concentration over the Southeast United States and over the Great Plains, consistent with climatological expectations for springtime convection. The distribution of maximum detected CTC values across all tracks (Figure 6) was notably right skewed. The mode of the distribution occurred at 13 K 5 min^{-1}, with the distribution gradually tapering off beyond ~15 K 5 min^{-1}. Only a small number of cases exceeded 20 K 5 min^{-1}, with the most extreme cooling observed at 32 K 5 min^{-1}. Statistical percentiles further characterize this distribution: the 25th percentile of maximum CTC was 13.44 K 5 min^{-1}, the median (50th percentile) was 15.28 K 5 min^{-1}, the 75th percentile was 18.15 K 5

min^{-1}, and the 90^{th} percentile reached 21.32 K 5 min^{-1}. These percentiles help to constrain typical DOF-based CTC intensity for DC events (which is helpful when designing color-scales to view CTC products in operations).

The distribution reveals that most CI cases occurred in environments with moderate to high instability, with the peak frequency centered at 2720 J kg^{-1} (Figure 7). This finding suggests that most CI events were embedded within atmospheres conducive to severe weather, as expected. Due to the stringent thresholds in the automated algorithm, fewer cases (12^{th} percentile) occurred in low-CAPE environments (i.e., <1000 J kg^{-1}). Most cases fell under strong CAPE regimes, between 1945 and 3500 J kg^{-1}. To complement the statistical analysis of the full dataset, this study also examines two individual CI cases in detail—one characterized by a high peak CTC and another by a lower peak CTC. These case studies were selected to illustrate the range of CTC behavior and its relationship to both ambient instability and subsequent storm development.

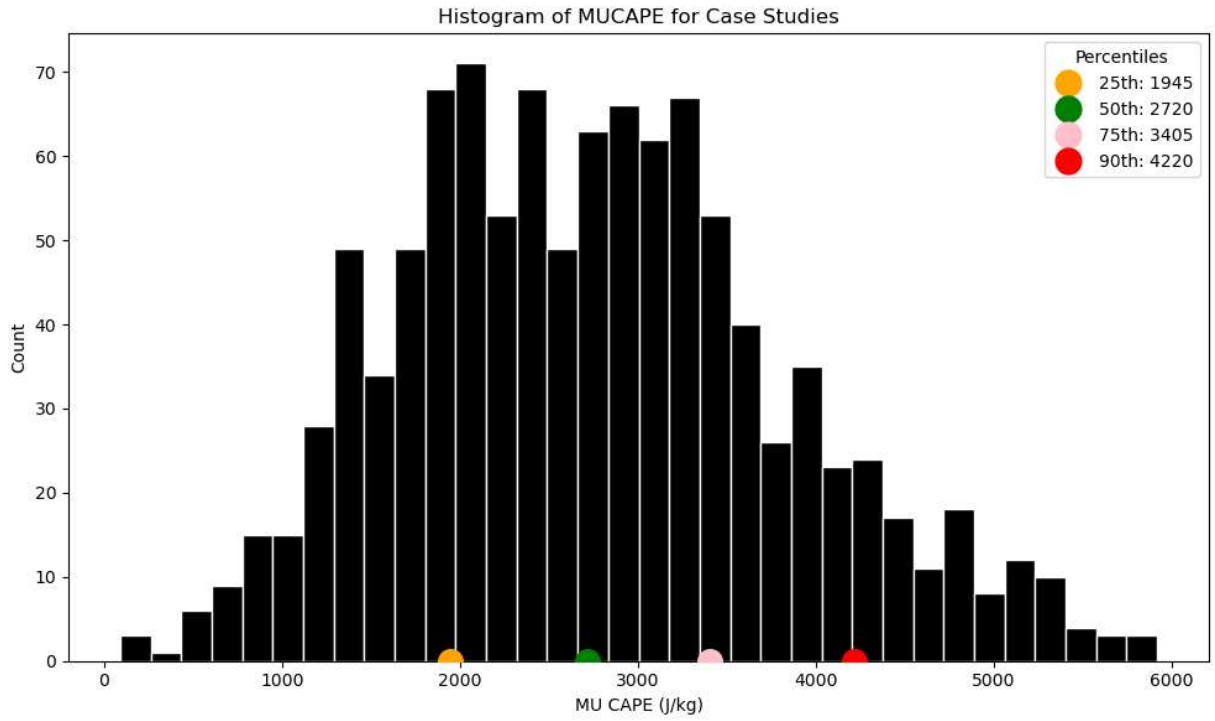

Figure 7: Histogram of the MUCAPE values associated with the 1,063 CI cases. The x-axis represents MUCAPE in joules per kilogram (J kg^{-1}), while the y-axis indicates the number of cases within each MUCAPE bin.

4.2 Addressing Science Question 1: How does CTC relate to ambient instability?

Figure 8 presents the CTC growth curves for two contrasting CI case studies: one with a weaker updraft, in southern North Carolina on 25 May 2024 (left panel) and one with a stronger updraft, in northern North Carolina, on 27 May 2024 (right panel). The weaker case, with a MUCAPE of 1730 J kg^{-1}, shows a modest peak CTC near 12 K 5 min^{-1} (below the 25th percentile identified in Figure 6). In contrast, the stronger case, with a MUCAPE of 3790 J kg^{-1}, exhibits a much more pronounced peak CTC, 21.5 K 5 min^{-1} (which is above the 75th percentile in this dataset). This contrast reinforces the broader trend observed in the full dataset: higher ambient instability tends to support stronger CTC signals, consistent with more vigorous vertical motion and latent heat release.

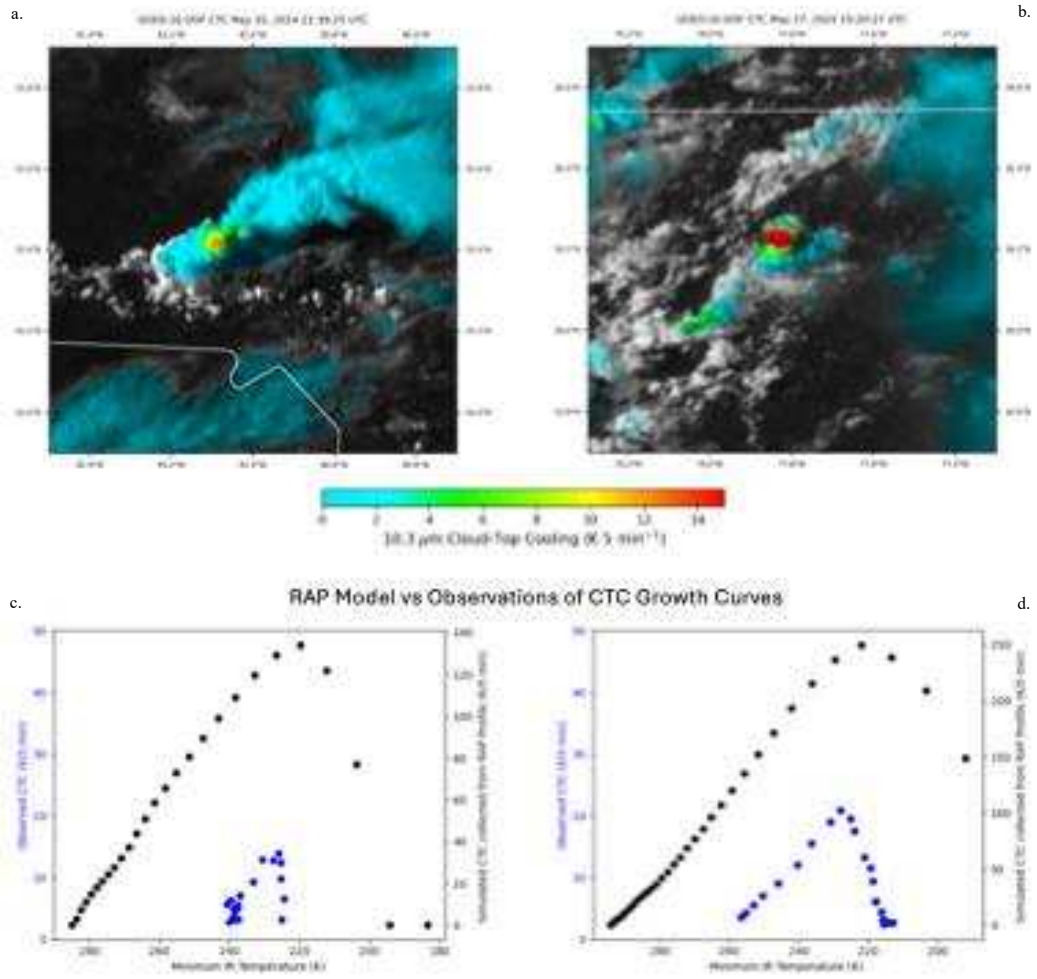

Figure 8: a) Weak CTC case study (maximum value 13 K 5 min^{-1}) from 25 May 2024 shown in the same sandwich format as Figure 2), with the red box indicating where CTC was objectively retrieved, shown with b) Strong CTC Study (Maximum Value 21 K 5 min^{-1}) from 27 May 2024, c) growth curves of the weak CTC case study, observed CTC and RAP CTC as a function of IR temperature, and d) growth curves of the strong CTC case study, observed CTC and RAP CTC as a function of IR temperature.

A key finding from these case studies is the systematic overstatement of CTC in the simulated RAP profiles compared to the observed satellite-derived CTC. This discrepancy was consistent across nearly all cases examined in this research. A primary cause of such is due to how CTC is observed via satellite tracking. Even with perfect tracking, we likely cannot observe the overturning of individual, undiluted parcels as they rise in the atmosphere (as was simulated with the RAP-based CAPE profile), due to the coarse spatial resolution of the satellite imagery and the fine spatial scale of these parcels. Rather, we approximate the growth by comparing the

evolving state of the DC cloud-tops containing a mixture of parcels over a large area growing at different rates. A reduction in magnitude may also indicate where processes not captured by parcel theory exist (i.e., entrainment or pressure gradient forces). Despite differences in magnitudes, the shape of the growth curves, including the locations of increasing versus decreasing CTC as a function of temperature, between observed and CAPE-simulated CTC were remarkably similar, implying a relationship exists between CTC observations and instability. While the two case studies illustrate how CTC behavior can vary with ambient instability, a broader statistical perspective is necessary to assess whether these patterns hold across a larger sample.

Box plots for the full dataset (1,063 cases) reveal a clear upward trend in maximum CTC with increasing CAPE (Figure 9). Median (as well as 25^{th} and 75^{th} percentile) CTC values rise progressively across the CAPE bins, indicating that stronger instability environments tend to support more intense CTC. This trend is consistent with the physical expectation that greater instability facilitates stronger updrafts and more rapid vertical cloud growth.

Notably, the spread of CTC values in Figure 9 also increases toward higher CAPE regimes, suggesting greater variability in convective response. This behavior could reflect the influence of additional factors such as entrainment or pressure-gradient forcing, which modulate how instability is realized in updraft development, though it also reflects how higher-CAPE environments can support more storms which grow with much stronger updrafts. The presence of outliers in each category further emphasizes the complexity of the CI process, while CAPE is a key ingredient, it is not the sole determinant of CTC strength (hence the relationship between the two is non-linear).

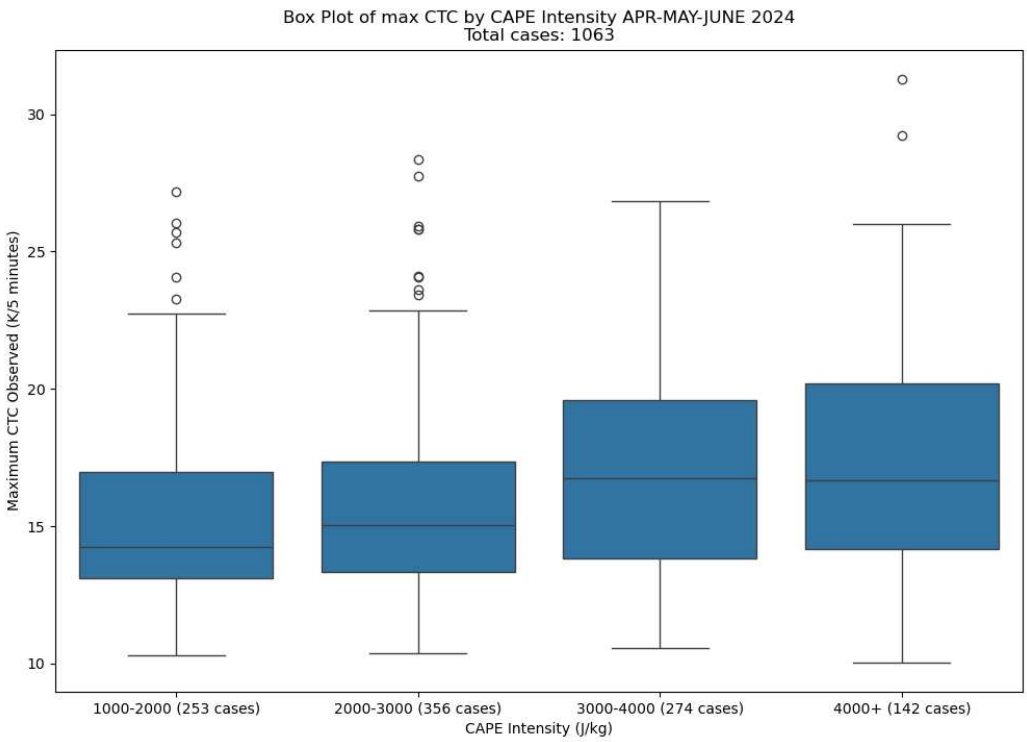

Figure 9: Box plots of Maximum CTC in different MUCAPE regimes for all case studies.

Interestingly, some storms notably also have moderate to high-CTC for several time steps. Such sustained growth is captured by integrating CTC with time over a 3 min window, which shows greater separation with increasing instability than peak CTC alone (Figure 10). This finding reinforces the earlier findings from maximum CTC analysis, while reducing possible retrieval-induced noise. Notably, the spread of values still increases in the higher CAPE categories, suggesting that while instability supports stronger integrated CTC, the actual manifestation of that potential is modulated by other factors that are not captured by CAPE and parcel theory, though higher CAPE environments can also support strong, sustained updrafts.

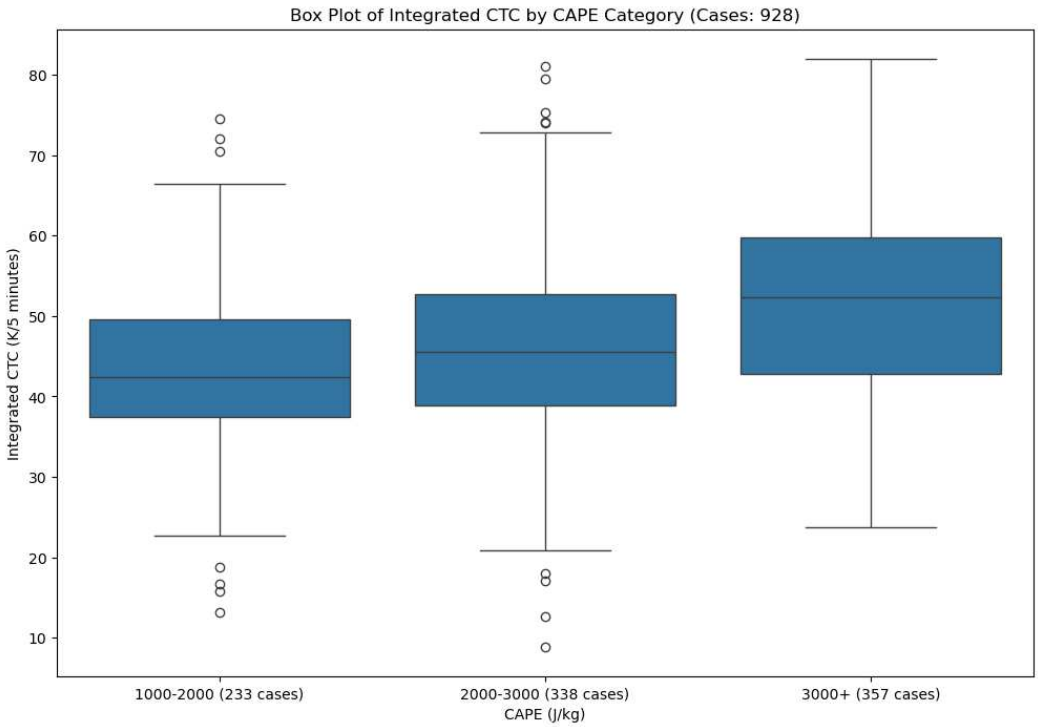

Figure 10: Box plots of integrated CTC in different MUCAPE regimes for case studies where Integrated CTC was able to be computed.

4.3 Addressing Science Question 2: How does CTC relate to the timing of storm severity?

Revisiting the two CTC cases discussed previously, the weak storm from 25 May 2024, and the strong storm from 27 May 2024, there are clear differences on how each storm intensifies (Figure 11). The strong CTC case shows a rapid progression from initial CTC detection to radar-observed storm severity, with only a 12 min delay between CTC onset and hail detection. The short lead time reflects a highly unstable environment (MUCAPE at 17.1st percentile) and a strong, sustained updraft, capable of rapidly producing large hailstones, and emphasized by the large and rapid increase in CTC values. In contrast, the weak case shows a longer progression from initial CTC detection to storm severity, with 33 min lead time before hail detection. This storm developed in a moderately unstable environment (MUCAPE at 83.5th percentile) and showed a weaker CTC signal, consistent with a slower and less vigorous updraft evolution.

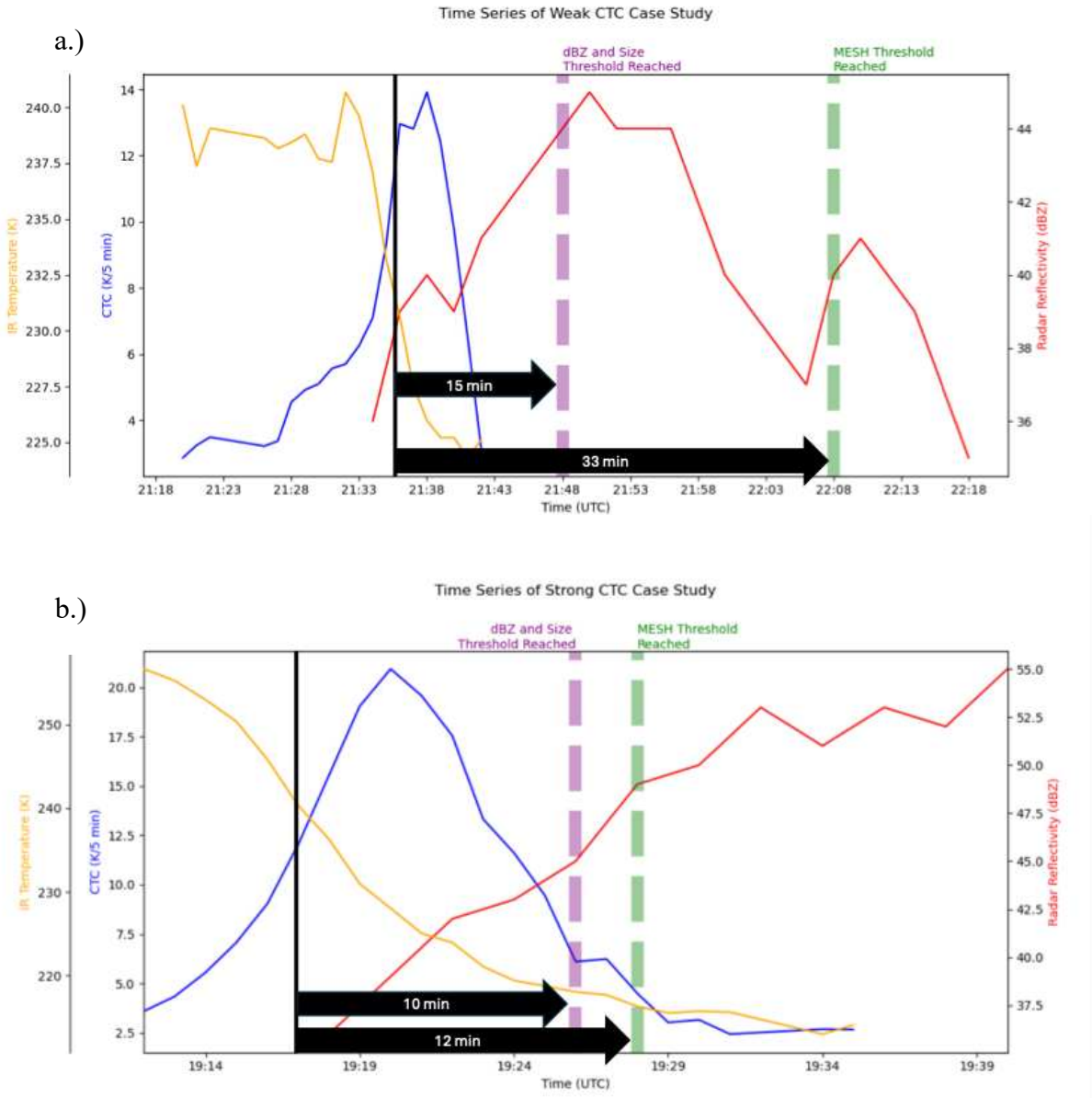

Figure 11: a) The time series of the weak CTC case study (Maximum Value 13 K 5 min^{-1}) from 25 May 2024 shown with b) the time series of the strong CTC case study (maximum value = 21 K 5 min^{-1}) from 27 May 2024. Blue line indicates CTC values, red line indicates MRMS reflectivity values at -10 °C isotherm, and orange line indicates 10.3 µm IR temperature values. Black line and arrows indicate time it took from initial CTC threshold of 12 K 5 min^{-1} to significant DC of 35 dBZ and 49 km^2 (purple dashed line) in size and severe DC of 1" in MESH (green dashed line).

When investigating the relationship between CTC and the timing of significant or severe weather, higher CTC led to more rapid formation of DC and subsequent phenomena (Figure 12). Significant CTC signals precede significant radar signals by ~17-20 min, which appears somewhat dependent on the strength of the initial updraft with shorter lead-times observed for updrafts with > 15 K 5 min^{-1} cooling. The median decreases across CTC categories, from 12-15 and > 15 K 5 min^{-1}, and especially for significant convection, the spread of lead times narrows as CTC strength increases. This relationship is evident in the tightening interquartile ranges and shorter whiskers in the higher CTC bins, particularly for severe convection. In other words, stronger CTC signals are associated with more consistent timing between satellite-detected cloud growth and radar-observed storm intensification. Weaker CTC events (12–15 K 5 min^{-1}) show greater variability in lead times, especially for severe convection, with a broader range and higher medians. This finding suggests that while weaker CTC can still precede severe outcomes, the timing is less predictable and more dependent on other environmental factors—an important consideration for operational forecasters in terms when and where to utilize CTC information with confidence. Among our dataset cases were several updrafts, especially in the 12-15 K 5 min^{-1} bin, that exceed lead times of 30 min, which indicates cells where the initial updraft was likely only part of a larger system that on a whole produced significant weather. All of these factors should calibrate how forecasters interpret >12 K 5 min^{-1} signals for decision making (e.g. issuing hail-based severe warnings).

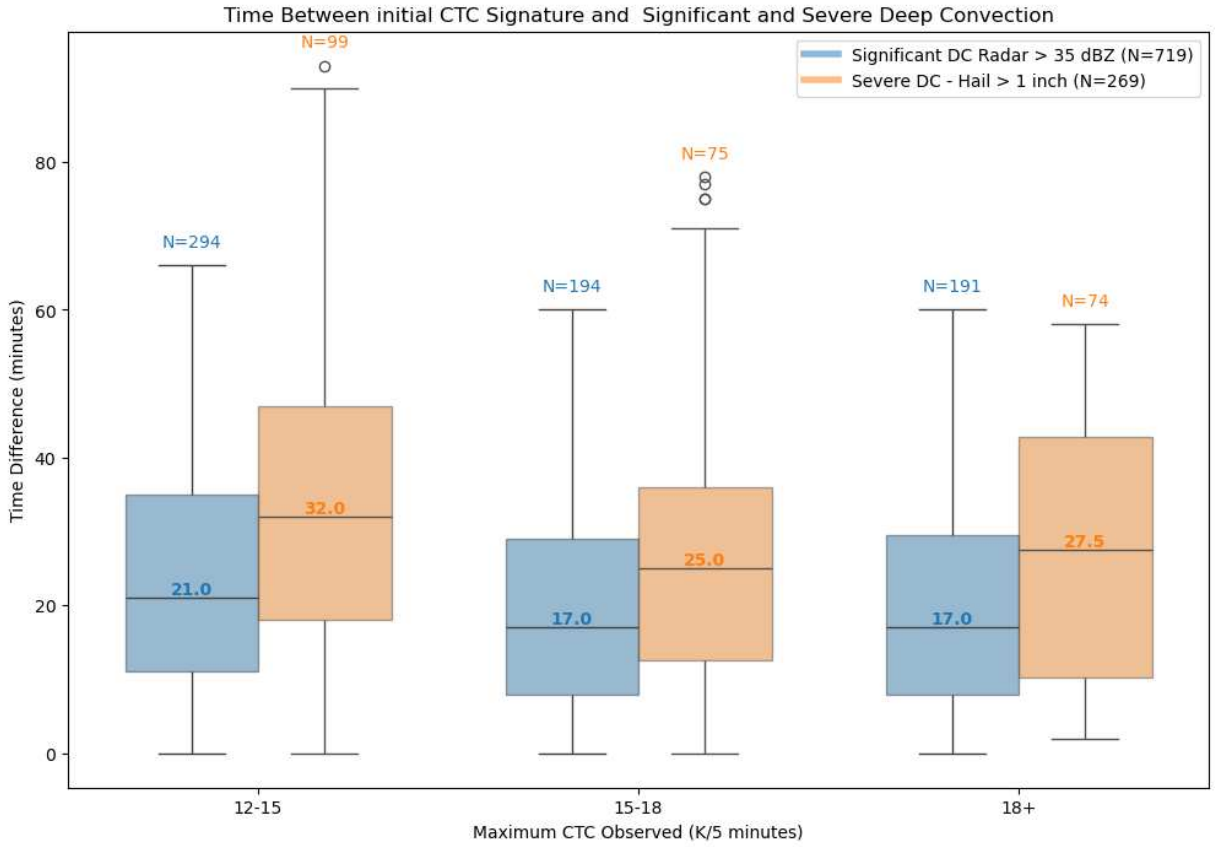

Figure 12: Lead times between the first instance of 12 K 5 min^{-1} CTC and reflectivity of 35 dBZ and 7 km in area thresholds, based on varying strengths of maximum CTC. N. is the number of cases in each bin

For storms reaching severe convection status, with MRMS MESH detecting > 1" diameter hail, the subset of 269 cases is smaller than the full dataset due to many storms (~75 % in this sample) not meeting the severe severity criteria. It is important to note that hail production is influenced by a large range of environmental characteristics beyond CTC strength alone. Factors such as storm-relative flow, freezing level height, mid-level lapse rates, and storm organization all play critical roles in determining whether hail forms and reaches the surface (Markowski and Richardson 2010).

Our results show that CTC precedes hail production by even greater lead times, closer to 25-32 min, with again shorter lead times for > 15 K 5 min^{-1} updrafts. Such long lead times imply

that the observed updrafts in satellite were not the only ones involved in hail production, and severe DC likely involved different, unobserved updrafts at later times to help produce the hail. Therefore, while CTC provides valuable insight into updraft vigor and storm evolution speed, it should be interpreted within the broader context of the storm evolution and environment. Although left as a topic for future research, these results in this sample suggest an observation that CTC strength is not only a marker of updraft intensity but also a predictor of storm evolution consistency. Stronger CTC events likely reflect more vigorous and organized vertical motion, leading to faster and more predictable development of radar-observable features such as precipitation cores and hail.

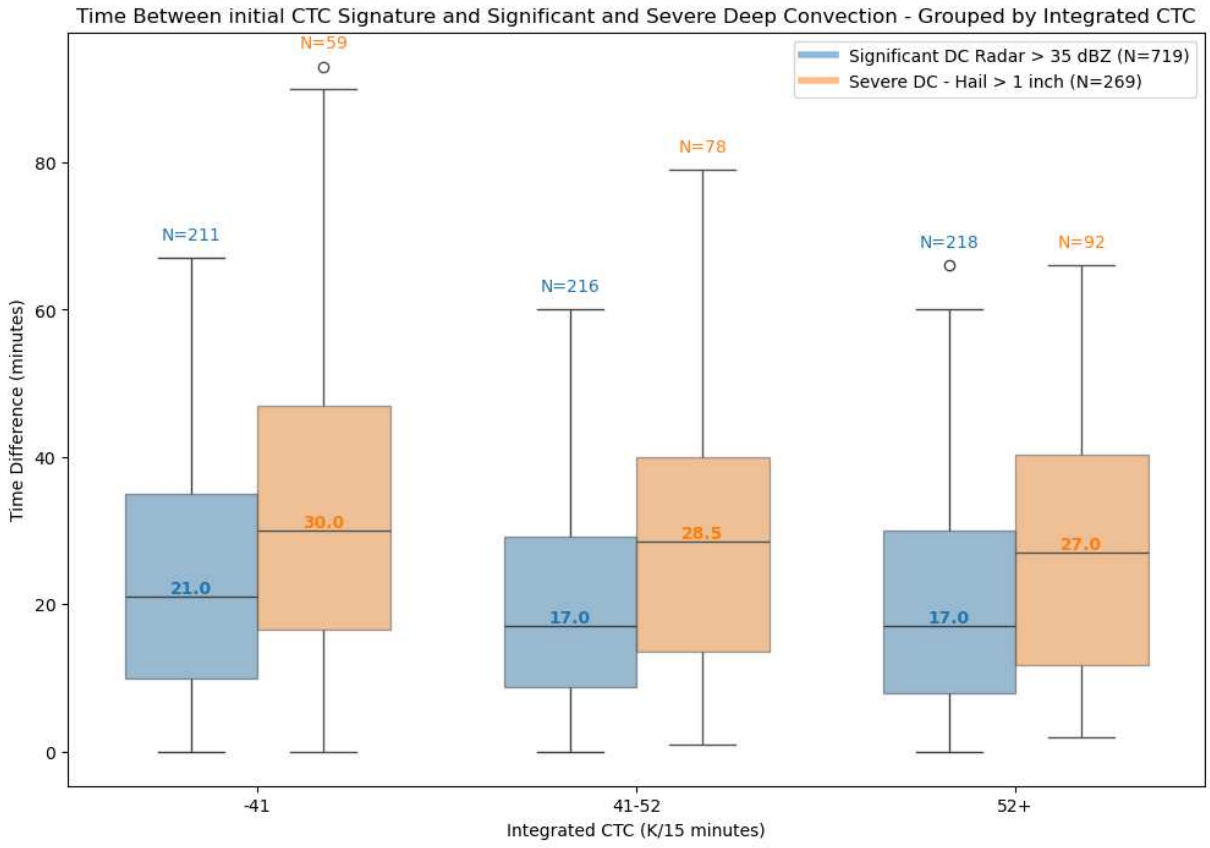

Figure 13: Lead times between first instance of 12 K 5 min^{-1} CTC and MRMS MESH Hail reaching greater than 1" in diameter, grouped by various strengths of CTC. N is the number of cases in each bin.

Figure 13 presents the same boxplots as Figure 12, relating between significant and severe DC, but now grouped by integrated CTC, a metric representing the highest rolling 3-minute sum of CTC values in each case study track. The integrated CTC values were binned using the 33rd and 66th percentiles of the dataset, resulting in three categories. For significant convection, the median lead time decreases from 20 min in the lowest bin to 17 min in the middle and highest bins. For severe convection, the median lead time also decreases, from 30 min in the lowest bin to 28.5 min in the middle bin and 27 min in the highest bin. While the median values show only modest decreases, the spread of lead times for the more extreme percentiles narrows with increasing integrated CTC, especially for severe convection. This suggests that higher integrated CTC values are associated with more consistent timing between CTC and the onset of severe weather, and points to integrated CTC as a potentially more robust application for operational forecasters to consider.

5 CONCLUSIONS AND FUTURE WORK

This research investigates the relationships between objectively retrieved CTC atop DC collected with an advanced DOF retrieval algorithm, the ambient environmental thermodynamics, and the timing of subsequent severe weather. By leveraging high-temporal-resolution satellite imagery, radar observations, and model-derived thermodynamic profiles, the study addressed two central questions:

1. How does DOF-based CTC relate to ambient instability?
2. How does DOF-based CTC relate to the timing of significant and severe deep convection?

The results demonstrated a positive correlation between stronger CTC signals and higher environmental instability, as measured by MUCAPE, though this relationship was found to be relatively non-linear. Case studies and composite analyses showed that storms developing in more unstable environments tended to support more intense and sustained CTC, consistent with stronger updrafts and more rapid vertical development. Additionally, stronger CTC signals were generally associated with shorter and more consistent lead times to radar-observed storm severity. Most CTC cases gave ~17-21 min lead time between the initial CTC signal and significant precipitation, and ~25-32 min lead time between the initial CTC signal and large hail occurrence (>1” diameter).

However, the analysis also revealed notable variability in the data. Boxplots of CTC versus CAPE and lead time distributions showed considerable spread, particularly in moderate CTC regimes. This noise may reflect a combination of factors, including limitations in the objective retrieval method, assumptions of updraft to thermodynamic relationships made in

parcel theory (which exclude entrainment and pressure gradient forcing), environmental heterogeneity, tracking uncertainties, and errors in CAPE representation made by NWP models. These findings highlight the complexity of convective development and the need for multi-parameter approaches in severe weather forecasting.

Despite the promise of DOF-based CTC to understand instability and the lead time before severe weather, several limitations must be acknowledged in this study, enumerated as follows:

1. The TOBAC tracking algorithm, while effective for object-based segmentation, may struggle with accurately capturing the full lifecycle of convective features, particularly in cases involving storm mergers or splits. These complexities can lead to discontinuities or misrepresentations in the tracking output.
2. Additionally, the CTC retrieval itself is sensitive to nearby cloud structures; overlapping or adjacent clouds can artificially enhance or suppress the observed cooling signal, leading to potential over- or underestimation of updraft strength. The choice of a 5-minute cooling rate (K 5 min^{-1}) may also limit temporal sensitivity—shorter intervals, such as 3-minute or 1-minute rates, could reveal more rapid changes and improve the timeliness of detection (at the cost of being more sensitive to retrieval noise).
3. This temporal resolution issue may also contribute to discrepancies observed when comparing RAP-derived parcel theory-based estimates of CTC to satellite observations, as the latter represent a spatially averaged signal from a cluster of parcels rather than a single, idealized updraft.
4. Furthermore, the RAP model itself is subject to known deficiencies in representing mesoscale thermodynamic environments, which could introduce additional uncertainty in the instability estimates.

Addressing these limitations may require comparisons to rawinsondes in future field campaigns that directly observe environmental thermodynamics in proximity to DC initiation, coupled with cloud-particle-resolving radars or lidars that allow real-time validation of satellite-derived CTC approximations of updraft growth and improved understanding of storm dynamics.

Building on the findings of this study, several avenues for future research are proposed to enhance the utility of satellite-based diagnostics in convective nowcasting, as follows:

1. First would be to explore the accuracy and ability to objectively retrieve CAPE using proxy atmospheric soundings and CTC alone.
2. Additional multi-spectral datasets can be collected to convert CTC into a more probabilistic nowcasting framework, such as SatCast or ProbSevere (which has yet to be accomplished due to the novelty of the DOF-based retrieval capabilities).
3. Another important extension of this work is the investigation of cloud-top warming, which may signal the weakening or dissipation of mature convection. Understanding the timing and spatial patterns of warming could provide valuable information about storm decay, helping forecasters anticipate when and where severe weather threats are diminishing. This would complement the current focus on initiation and intensification, offering a more complete picture of the convective lifecycle.

This research underscores the value of developing innovative satellite-based tools to enhance the early detection and characterization of severe DC storms. By applying cutting-edge DOF-based techniques to the challenge of observing convective growth, this study takes an important step toward improving the lead time and understanding of severe weather environments. The demonstrated relationships between CTC, environmental instability, and

storm severity highlight the potential of satellite-derived diagnostics to complement traditional forecasting methods. Looking ahead, the next generation of geostationary satellites, such as NOAA's GeoXO series, promises to further advance these capabilities. With its enhanced spatial resolution (0.25 km in the visible and 1.0 km in the IR), GeoXO will offer unprecedented detail in cloud-top observations, enabling more precise tracking of convective evolution and potentially unlocking new insights into storm dynamics. As these tools mature, they hold exciting promise for operational meteorology, empowering forecasters with earlier, more accurate guidance to anticipate and mitigate the hazards posed by severe weather.

6 REFERENCES

Adler, R. F., and D. D. Fenn, 1979: Thunderstorm Intensity as Determined from Satellite Data. *Journal of Applied Meteorology*, **18**, 502–517, https://doi.org/10.1175/1520-0450(1979)018<0502:TIADFS>2.0.CO;2.

Apke, J. M., and J. R. Mecikalski, 2021: On the origin of rotation derived from super rapid scan satellite imagery at the cloud tops of severe deep convection. *Mon Weather Rev*, **149**, 1827–1851, https://doi.org/10.1175/MWR-D-20-0209.1.

——, ——, and C. P. Jewett, 2016: Analysis of mesoscale atmospheric flows above mature deep convection using super rapid scan geostationary satellite data. *J Appl Meteorol Climatol*, **55**, 1859–1887, https://doi.org/10.1175/JAMC-D-15-0253.1.

——, ——, K. Bedka, E. W. Mccaul, C. R. Homeyer, and C. P. Jewett, 2018: Relationships between deep convection updraft characteristics and satellite-based super rapid scan mesoscale atmospheric motion vector-derived flow. *Mon Weather Rev*, **146**, 3461–3480, https://doi.org/10.1175/MWR-D-18-0119.1.

——, K. A. Hilburn, S. D. Miller, and D. A. Peterson, 2020: Towards objective identification and tracking of convective outflow boundaries in next-generation geostationary satellite imagery. *Atmos Meas Tech*, **13**, 1593–1608, https://doi.org/10.5194/amt-13-1593-2020.

——, Y. J. Noh, and K. Bedka, 2022: Comparison of Optical Flow Derivation Techniques for Retrieving Tropospheric Winds from Satellite Image Sequences. *J Atmos Ocean Technol*, **39**, 2005–2021, https://doi.org/10.1175/JTECH-D-22-0057.1.

Bedka, K. M., and J. R. Mecikalski, 2005: Application of Satellite-Derived Atmospheric Motion Vectors for Estimating Mesoscale Flows. *Journal of Applied Meteorology*, **44**, 1761–1772, https://doi.org/10.1175/JAM2264.1.

Benjamin, S. G., and Coauthors, 2016: A North American Hourly Assimilation and Model Forecast Cycle: The Rapid Refresh. *Mon Weather Rev*, **144**, 1669–1694, https://doi.org/10.1175/MWR-D-15-0242.1.

Cintineo, J. L., M. J. Pavolonis, J. M. Sieglaff, and D. T. Lindsey, 2014: An empirical model for assessing the severe weather potential of developing convection. *Weather Forecast*, **29**, 639–653, https://doi.org/10.1175/WAF-D-13-00113.1.

——, and Coauthors, 2018: The NOAA/CIMSS ProbSevere model: Incorporation of total lightning and validation. *Weather Forecast*, **33**, 331–345, https://doi.org/10.1175/WAF-D-17-0099.1.

——, M. J. Pavolonis, J. M. Sieglaff, L. Cronce, and J. Brunner, 2020: NOAA ProbSevere v2.0—ProbHail, ProbWind, and ProbTor. *Weather Forecast*, **35**, 1523–1543, https://doi.org/10.1175/WAF-D-19-0242.1.

——, ——, and ——, 2022: ProbSevere LightningCast: A Deep-Learning Model for Satellite-Based Lightning Nowcasting. *Weather Forecast*, **37**, 1239–1257, https://doi.org/10.1175/WAF-D-22-0019.1.

Dixon, M., and G. Wiener, 1993: TITAN: Thunderstorm Identification, Tracking, Analysis, and Nowcasting—A Radar-based Methodology. *J Atmos Ocean Technol*, **10**, 785–797, https://doi.org/10.1175/1520-0426(1993)010<0785:TTITAA>2.0.CO;2.

Feltz, M. L., L. Borg, R. O. Knuteson, D. Tobin, H. Revercomb, and A. Gambacorta, 2017: Assessment of NOAA NUCAPS upper air temperature profiles using COSMIC GPS radio occultation and ARM radiosondes. *Journal of Geophysical Research: Atmospheres*, **122**, 9130–9153, https://doi.org/10.1002/2017JD026504.

Fortun, D., P. Bouthemy, and C. Kervrann, 2015: Optical flow modeling and computation: A survey. *Computer Vision and Image Understanding*, **134**, 1–21, https://doi.org/10.1016/j.cviu.2015.02.008.

Hartung, D. C., J. M. Sieglaff, L. M. Cronce, and W. F. Feltz, 2013: An intercomparison of UW cloud-top cooling rates with WSR-88D radar data. *Weather Forecast*, **28**, 463–480, https://doi.org/10.1175/WAF-D-12-00021.1.

Hasler, A. F., J. Strong, R. H. Woodward, and H. Pierce, 1991: Automatic Analysis of Stereoscopic Satellite Image Pairs for Determination of Cloud-Top Height and Structure. *Journal of Applied Meteorology*, **30**, 257–281, https://doi.org/10.1175/1520-0450(1991)030<0257:AAOSSI>2.0.CO;2.

Heidinger, A., Y. Li, and S. Wanzong, 2020: Enterprise AWG Cloud Height Algorithm (ACHA). *NOAA NESDIS CENTER for SATELLITE APPLICATIONS and RESEARCH*. Accessed 10 June 2025, https://www.star.nesdis.noaa.gov/jpss/documents/ATBD/ATBD_EPS_Cloud_ACHA_v3.4.pdf.

Horn, B. K. P., and B. G. Schunck, 1981: Determining Optical Flow. *Artif Intell*, **17**, 185–203, https://doi.org/https://doi.org/10.1016/0004-3702(81)90024-2.

Lakshmanan, V., and T. Smith, 2010: An Objective Method of Evaluating and Devising Storm-Tracking Algorithms. *Weather Forecast*, **25**, 701–709, https://doi.org/10.1175/2009WAF2222330.1.

Line, W. E., T. J. Schmit, D. T. Lindsey, and S. J. Goodman, 2015: Use of Geostationary Super Rapid Scan Satellite Imagery by the Storm Prediction Center*. *Weather Forecast*, **31**, 483–494, https://doi.org/10.1175/10.1175/WAF-D-15-0135.s1.

Mack, R. A., A. F. Hasler, and R. F. Adler, 1983: Thunderstorm Cloud Top Observations Using Satellite Stereoscopy. *Mon Weather Rev*, **111**, 1949–1964, https://doi.org/10.1175/1520-0493(1983)111<1949:TCTOUS>2.0.CO;2.

Markowski, P., and Y. Richardson, 2010: *Mesoscale Meteorology in Midlatitudes*. 1st ed. Wiley-Blackwell.

Mecikalski, J. R., and K. M. Bedka, 2006: Forecasting Convective Initiation by Monitoring the Evolution of Moving Cumulus in Daytime GOES Imagery. *Mon Weather Rev*, **134**, https://doi.org/https://doi.org/10.1175/MWR3062.1.

Mecikalski, J. R., C. P. Jewett, J. M. Apke, and L. D. Carey, 2016: Analysis of cumulus cloud updrafts as observed with 1-min resolution super rapid scan GOES imagery. *Mon Weather Rev*, **144**, 811–830, https://doi.org/10.1175/MWR-D-14-00399.1.

——, T. N. Sandmæl, E. M. Murillo, C. R. Homeyer, K. M. Bedka, J. M. Apke, and C. P. Jewett, 2021: Random Forest Model to Assess Predictor Importance and Nowcast Severe Storms using High-Resolution Radar–GOES Satellite–Lightning Observations. *Mon Weather Rev*, **149**, 1725–1746, https://doi.org/10.1175/MWR-D-19-0274.1.

NOAA National Centers for Environmental Information (NCEI), 2025: U.S. Billion-Dollar Weather and Climate Disasters , https://doi.org/10.25921/stkw-7w73.

Ortland, S. M., M. J. Pavolonis, and J. L. Cintineo, 2023: The Development and Initial Capabilities of ThunderCast, a Deep Learning Model for Thunderstorm Nowcasting in the United States. *Artificial Intelligence for the Earth Systems*, **2**, 1–17, https://doi.org/10.1175/AIES-D.

Ouyed, A., X. Zeng, L. Wu, D. Posselt, and H. Su, 2021: Two-Stage Artificial Intelligence Algorithm for Calculating Moisture-Tracking Atmospheric Motion Vectors. *J Appl Meteorol Climatol*, **60**, 1671–1684, https://doi.org/10.1175/JAMC-D-21-0070.1.

Petty, G., 2008: *A First Course in Atmospheric Thermodynamics*. 1st ed. Sundog Publishing .

Roberts, R. D., and S. Rutledge, 2002: Nowcasting Storm Initiation and Growth Using GOES-8 and WSR-88D Data. *Weather Forecast*, **18**, 562–584.

Scarino, B., K. Itterly, K. Bedka, C. R. Homeyer, J. Allen, S. Bang, and D. Cecil, 2023: Deriving Severe Hail Likelihood from Satellite Observations and Model Reanalysis Parameters Using a Deep Neural Network. *Artificial Intelligence for the Earth Systems*, **2**, https://doi.org/10.1175/AIES-D-22-0042.1.

Schmit, T. J., P. Griffith, M. M. Gunshor, J. M. Daniels, S. J. Goodman, and W. J. Lebair, 2017: A Closer Look at the ABI on the GOES-R Series. *Bull Am Meteorol Soc*, **98**, 681–698, https://doi.org/10.1175/BAMS-D-15-00230.1.

Sieglaff, J. M., L. M. Cronce, W. F. Feltz, K. M. Bedka, M. J. Pavolonis, and A. K. Heidinger, 2011: Nowcasting convective storm initiation using satellite-based box-averaged cloud-top cooling and cloud-type trends. *J Appl Meteorol Climatol*, **50**, 110–126, https://doi.org/10.1175/2010JAMC2496.1.

——, ——, and ——, 2014: Improving satellite-based convective cloud growth monitoring with visible optical depth retrievals. *J Appl Meteorol Climatol*, **53**, 506–520, https://doi.org/10.1175/JAMC-D-13-0139.1.

Smith, T. M., and Coauthors, 2016: Multi-Radar Multi-Sensor (MRMS) Severe Weather and Aviation Products: Initial Operating Capabilities. *Bull Am Meteorol Soc*, **97**, 1617–1630, https://doi.org/10.1175/BAMS-D-14-00173.1.

Sokolowsky, G. A., and Coauthors, 2024: *tobac* v1.5: introducing fast 3D tracking, splits and mergers, and other enhancements for identifying and analysing meteorological phenomena. *Geosci Model Dev*, **17**, 5309–5330, https://doi.org/10.5194/gmd-17-5309-2024.

Stettner, D., C. Velden, R. Rabin, S. Wanzong, J. Daniels, and W. Bresky, 2019: Development of Enhanced Vortex-Scale Atmospheric Motion Vectors for Hurricane Applications. *Remote Sens (Basel)*, **11**, 1981, https://doi.org/10.3390/rs11171981.

Vandal, T. J., K. Duffy, W. McCarty, A. Sewnath, and R. Nemani, 2022: Dense Feature Tracking of Atmospheric Winds with Deep Optical Flow. *Proceedings of the 28th ACM SIGKDD Conference on Knowledge Discovery and Data Mining*, New York, NY, USA, ACM, 1807–1815, https://doi.org/10.1145/3534678.3539345.

Velden, C., and Coauthors, 2005: Recent Innovations in Deriving Tropospheric Winds from Meteorological Satellites. *Bull Am Meteorol Soc*, **86**, 205–224, https://doi.org/10.1175/BAMS-86-2-205.

Wylie, D. P., D. Santek, D. O', and C. Starr, 1998: Cloud-Top Heights from GOES-8 and GOES-9 Stereoscopic Imagery. *J Appl Meteorol Climatol*, **37**, 405–413.

Yanovsky, I., D. J. Posselt, L. Wu, and S. Hristova-Veleva, 2024: Quantifying Uncertainty in Atmospheric Winds Retrieved from Optical Flow: Dependence on Weather Regime. *J Appl Meteorol Climatol*, **63**, 1113–1135, https://doi.org/10.1175/JAMC-D-23-0169.1.

Zimmer, H., A. Bruhn, and J. Weickert, 2011: Optic Flow in Harmony. *Int J Comput Vis*, **93**, 368–388, https://doi.org/10.1007/s11263-011-0422-6.